

Structural, electronic and magnetic properties ofFe-doped strontium ruthenates

Nan Liu(刘楠), Xiao-Chao Wang(王晓超), and Liang Si(司良)
Citation: Chin. Phys. B, 2023, 32 (**11**): 117101. DOI: 10.1088/1674-1056/ad0112
Journal homepage: http://cpb.iphy.ac.cn; http://iopscience.iop.org/cpb

What follows is a list of articles you may be interested in

Design of sign-reversible Berry phase effect in 2D magneto-valley material

Yue-Tong Han(韩曰通), Yu-Xian Yang(杨宇贤), Ping Li(李萍), and Chang-Wen Zhang(张昌文)
Chin. Phys. B, 2023, 32 (**9**): 097101. DOI: 10.1088/1674-1056/acd920

Highly anisotropic Dirac fermion and spin transportproperties in Cu-graphane

Chao Wu(吴超), Lichuan Zhang(张礼川), Lin Xia(夏霖), Dong Hao(郝东), Shiqi Li(李仕琪), Lizhi Zhang(张礼智), Yuee Xie(谢月娥), and Yuanping Chen(陈元平)
Chin. Phys. B, 2023, 32 (**8**): 087104. DOI: 10.1088/1674-1056/accff1

Modulation of CO adsorption on 4,12,2-graphyne by Fe atom doping and applied electric field

Yu Dong(董煜), Zhi-Gang Shao(邵志刚), Cang-Long Wang(王苍龙), and Lei Yang(杨磊)
Chin. Phys. B, 2023, 32 (**8**): 087101. DOI: 10.1088/1674-1056/acc935

High-temperature ferromagnetism and strong π-conjugation feature in two-dimensional manganese tetranitride

Ming Yan(闫明), Zhi-Yuan Xie(谢志远), and Miao Gao(高淼)
Chin. Phys. B, 2023, 32 (**3**): 037104. DOI: 10.1088/1674-1056/acae7b

Prediction of one-dimensional CrN nanostructure as a promising ferromagnetic half-metal

Wenyu Xiang(相文雨), Yaping Wang(王亚萍), Weixiao Ji(纪维霄), Wenjie Hou(侯文杰),Shengshi Li(李胜世), and Peiji Wang(王培吉)
Chin. Phys. B, 2023, 32 (**3**): 037103. DOI: 10.1088/1674-1056/acb200

SPECIAL TOPIC — Celebrating the 100th Anniversary of Physics Discipline of Northwest University

Structural, electronic and magnetic properties of Fe-doped strontium ruthenates

Nan Liu(刘楠)[1], Xiao-Chao Wang(王晓超)[1], and Liang Si(司良)[1,2,†]

[1] *School of Physics, Northwest University, Xi'an* 710127, *China*
[2] *Institute of Solid State Physics, TU Wien, Vienna* 1040, *Austria*

(Received 19 September 2023; revised manuscript received 7 October 2023; accepted manuscript online 7 October 2023)

By employing a combined approach of density-functional theory (DFT) and dynamical mean-field theory (DMFT) calculations, we examine the structural, electronic, and magnetic characteristics of two distinct strontium ruthenates: Sr_2RuO_4, an unconventional superconductor, and the correlated metal $SrRuO_3$, both at 50% Fe-doping level. In both $Sr_2Fe_{0.5}Ru_{0.5}O_4$ and $SrFe_{0.5}Ru_{0.5}O_3$, the original ruthenium (Ru) and the dopant iron (Fe) atoms adopt 3-dimensional and 2-dimensional G-type structures, respectively. The hybridization between Fe-3d and Ru-4d is comparatively weaker than in other double perovskite systems. The interplay between strong correlations and reduced itinerancy results in significant spin splitting at Fe and Ru sites. Consequently, a charge transfer process, along with the super-exchange effect, leads to antiferromagnetically coupled Fe^{3+} and Ru^{5+} ions and establishes a semiconducting ferrimagnetic order. Subsequent DMFT calculations demonstrate the persistence of the ferrimagnetic order even at room temperature (300 K). These findings align with prior reports on $SrFe_{0.5}Ru_{0.5}O_3$, thus reinforcing the notion that 3d–4d transition metal oxides hold considerable promise as candidates for high-performance spintronic devices, such as spin-valve sensors and spintronic giant magnetoresistance devices.

Keywords: first-principles calculations, double perovskites, correlation effects, dynamical mean-field theory

PACS: 71.15.Mb, 71.27.+a, 74.25.Ha, 75.50.Gg **DOI:** 10.1088/1674-1056/ad0112

1. Introduction

Perovskites oxides[1,2] have emerged as key players in hosting a wide range of exotic physical phenomena, including high-T_C superconductivity,[3] ferroelectricity[4,5] and Mott-insulator transition.[6,7] Among these oxides, strontium ruthenate stands out as one of the most extensively investigated strongly correlated perovskite materials due to its remarkable physical properties.[8,9] Two significant classes of ruthenates, namely (double) perovskites $SrRuO_3$ ($SrRuBO_6$) and Ruddlesden–Popper-type layered $Sr_{n+1}Ru_nO_{3n+1}$, have recently gained prominence as promising candidates for various technological applications. The intricate interplay among crystal distortions, lattice effects, spin and orbital degrees of freedom, electronic correlations, and spin–orbital coupling in $SrRuO_3$ and Sr_2RuO_4 gives rise to extraordinary physical states. These include anomalous Hall effects and the presence of magnetic monopoles,[10] skyrmion states,[11–14] and unconventional chiral p-wave superconductivity, along with other fascinating properties.[9,15–19] However, due to the moderately strong correlations of Ru-4d orbitals, the observability of the important physical phenomena in ruthenates is limited compared to the 3d transition metal oxides (TMOs). For instance, the ferromagnetic Curie temperature in perovskite $SrRuO_3$ is around 150 K–160 K,[8] and the critical temperature for superconductivity in Sr_2RuO_4 is approximately 1 K.[9]

In comparison to 4d and 5d TMOs, 3d TMOs consistently exhibit higher Curie or Néel temperatures. Examples include Fe_2O_3,[20] $LaFeO_3$,[21] and $La_{2/3}Sr(Ca)_{1/3}MnO_3$.[22] Previous experimental studies have shown that incorporating chemical doping techniques with (double) perovskite structures can lead to the development of new materials with novel properties, making them highly desirable for various technological applications.[23,24] Consequently, the physical properties of both $SrRuO_3$ and Sr_2RuO_4 have been found to be sensitive to material engineering techniques such as chemical doping,[25–28] strain,[29] and external field effects.[30,31] By manipulating these factors, modifications to the electronic structure and magnetic ordering in ruthenates can be induced. This includes the emergence of magnetic competition,[32] reshaping of electronic states $N(E_f)$ near the Fermi level,[33–35] occurrence of crystal orthorhombic distortion,[25,36] and positioning of the Fermi surface in closer proximity to the Van Hove singularity of the γ-band.[37] These controls allow for the fine-tuning of the electronic and magnetic properties in ruthenates, offering opportunities for tailoring materials for specific applications.

The magnetic transition and operational temperature of 4d transition metal oxides (TMOs), such as ruthenates, can be

†Corresponding author. E-mail: siliang@nwu.edu.cn

© 2023 Chinese Physical Society and IOP Publishing Ltd

naturally expected to be enhanced by the controlled incorporation of 3d transition metal dopants like Fe. The doping concentration can be precisely regulated by adjusting the doping amount and processing parameters. In the context of epitaxial growth of perovskite oxides, Fe doping refers to the intentional addition of iron (Fe) atoms to the *B*-site of ABO_3 perovskite oxide materials. Various methods, such as solid-state reactions and atomic layer deposition, can be employed to achieve Fe doping. Furthermore, Fe doping is anticipated to induce charge transfer phenomena[38] between Fe-3d and Ru-4d orbitals, resulting in unexpected exotic phenomena.[39] Due to the difference in electronegativity, electrons from the Ru-4d orbitals are expected to transfer to Fe-3d states, leading to the formation of Fe-$3d^5$ and Ru-$4d^3$ configurations.[40] This sets the stage for possible interactions between the possible high-spin Fe and Ru sites. Therefore, conducting further investigations into the electronic and magnetic structures of heavily Fe-doped $SrRuO_3$ and Sr_2RuO_4 holds crucial importance and offers fundamental insights into these systems.

This study aims to investigate the structural, magnetic, and electronic properties, as well as correlation effects of heavy Fe-doping in $SrRuO_3$ and Sr_2RuO_4 through DFT and DMFT calculations. We present a comparative analysis of the structural, electronic, and magnetic characteristics of both systems. The introduced Fe atoms are found to be distributed separately within $SrRuO_3$ and Sr_2RuO_4. DFT + U calculations reveal a weakened hybridization between Fe-3d and Ru-4d orbitals, leading to a significant charge transfer from Ru to Fe. Consequently, the Fe atoms adopt a Fe^{3+} state while the Ru atoms adopt a Ru^{5+} state. The presence of electronic correlations within both Fe-3d and Ru-4d orbitals results in substantial magnetic moments, giving rise to strong superexchange effect and the formation of ferrimagnetic (FIM) orders in $SrFe_{0.5}Ru_{0.5}O_3$ and $Sr_2Fe_{0.5}Ru_{0.5}O_4$. The Hund's exchange interaction plays a crucial role in the establishment of high-spin states for both Fe^{3+} and Ru^{5+} ions. To account for dynamical correlation effects, DFT + DMFT calculations are further performed, demonstrating that the FIM states in $SrFe_{0.5}Ru_{0.5}O_3$ and $Sr_2Fe_{0.5}Ru_{0.5}O_4$ persist even at room temperature.

2. Method

DFT structural relaxations are performed to reach the ground state structures for $SrFe_{0.5}Ru_{0.5}O_3$ and $Sr_2Fe_{0.5}Ru_{0.5}O_4$. After obtaining the ground structures with lowest DFT total energy, static calculations of band, density-of-states (DOS) are performed using the VASP[41,42] and WIEN2K[43,44] codes with the Perdew–Burke–Ernzerhof version of the generalized gradient approximation (GGA-PBE)[45] and a dense $11 \times 11 \times 11$ k-mesh for the $2 \times 2 \times 2$ supercell of $SrFe_{0.5}Ru_{0.5}O_3$ (Figs. 1(a)–1(d)), and a $6 \times 6 \times 3$ k-mesh for the $\sqrt{2} \times \sqrt{2} \times 1$ supercell of $Sr_2Fe_{0.5}Ru_{0.5}O_4$ (Figs. 1(e)–1(k)). In VASP calculations, we consider the following electron configurations as valence electrons: Sr $4s^24p^65s^2$, Ru $5s^14d^7$, Fe $4s^13d^7$, and O $2s^22p^4$. Correlation effects in Fe-3d and Ru-4d orbitals are considered by employing DFT + U method,[46,47] the interaction parameters for Fe-3d and Ru-4d are intra-orbital $U(\text{Fe}) = 5.0$ eV, Hund's exchange $J(\text{Fe}) = 0.5$ eV, inter-orbital $V(\text{Fe}) = U - 2J = 4.0$ eV; $U(\text{Ru}) = 3.0$ eV, $J(\text{Ru}) = 0.3$ eV, $V(\text{Ru}) = 2.4$ eV. These parameters are obtained from constrained random phase approximation (cRPA)[48] and agree with previous studies and have been proved effective for reproducing experimental observations,[49,50] e.g., the helical spin order consistent with experiments on $SrFeO_3$.[51]

As an input for the DMFT calculations, a low-energy effective Hamiltonian is generated by projecting the Fe-3d + Ru-4d derived DFT bands computed by WIEN2K around the Fermi level onto Wannier functions[52,53] using WIEN2WANNIER.[54,55] These are supplemented by a local density–density and Kanamori interaction, respectively. We employ the fully localized limit as a double counting correction scheme.[46] We solve the resulting many-body Hamiltonian from 100 K to 300 K within employing a continuous-time quantum Monte Carlo solver in the hybridization expansions[56] using W2DYNAMICS.[57,58] Real-frequency spectra are obtained with the ANA_CONT code[59] via analytic continuation using the maximum entropy method (MaxEnt).[60,61]

3. Results and discussion

3.1. Structural properties

To explore all possible structures for double-perovskite type (DP) $SrFe_{0.5}Ru_{0.5}O_3$ and Ruddlesden–Popper type (RP) $Sr_2Fe_{0.5}Ru_{0.5}O_4$, we list the possible structures in Figs. 1(a)–1(k) and Table 1 provides a summary of the (non-spin-polarized) DFT total energy and the corresponding space group. As shown in Table 1, the G-type structure, where the doped Fe atoms are separated by Ru atoms, exhibits the lowest energy state for both DP $SrFe_{0.5}Ru_{0.5}O_3$ (Fig. 1(h)) and RP $Sr_2Fe_{0.5}Ru_{0.5}O_4$ (Fig. 1(d)). These results indicate that in $SrRuO_3$ and Sr_2RuO_4, the doped Fe atoms tend to be separated (G-type order) rather than forming atomic clusters or exhibiting antisite disorder.[62] However, achieving a high-quality film of pure G-type double perovskites (DP) $SrFe_{0.5}Ru_{0.5}O_3$ or RP $Sr_2Fe_{0.5}Ru_{0.5}O_4$ may pose challenges due to potential antisite disorder.[62] Previous experiments have indicated

that Sr_2FeRuO_6 may exhibit spin-glass behavior[63,64] or long-range room-temperature magnetism[40] when the Ru and Fe ions are randomly distributed or when a perfect double perovskite structure is synthesized.

The relaxed in-plane lattice constants for DP $SrFe_{0.5}Ru_{0.5}O_3$ and RP $Sr_2Fe_{0.5}Ru_{0.5}O_4$ are found to be 7.758 Å (Fig. 1(h)) and 5.384 Å (Fig. 1(d)), respectively. In terms of pseudocubic coordination, these correspond to 3.879 Å and 3.807 Å, respectively. These values are comparable to the in-plane lattice constants of $SrVO_3$ (3.890 Å), $SrTiO_3$ (3.905 Å), and $LaAlO_3$ (3.778 Å). The similarity in lattice constants suggests the possibility of epitaxial growth and highlights the potential of these materials for applications in oxide devices.

Table 1. Relative total energies, space group of different phases of DP $SrFe_{0.5}Ru_{0.5}O_3$ and RP $Sr_2Fe_{0.5}Ru_{0.5}O_4$ computed by DFT, the unit is in meV of per $2\times2\times2$ supercell of $SrFe_{0.5}Ru_{0.5}O_3$ (e.g., Figs. 1(e)–1(k)) and $2\times2\times1$ supercell of $Sr_2Fe_{0.5}Ru_{0.5}O_4$ (Figs. 1(a) and 1(d)), respectively. The energy of the G-type for all systems is set as zero for comparison. To demonstrate the stability and validity of the GGA-PBE, the same calculations with LDA functional are also shown.

DP (GGA-PBE)	A	C1	C2	G
Space group	*P*4/*mmm* (123)	*P*4/*mmm* (123)	$P4_2/mmc$ (131)	*Fm*-3*m* (225)
Energy	312.2	337.5	405.5	0
DP (GGA-PBE)	D-1	D-2	D-3	–
Space group	*P*4/*mmm* (123)	$P4_2/mmc$ (131)	*Pm*-3*m* (221)	–
Energy	294.1	415.7	318.6	–
RP (GGA-PBE)	A	C1	C2	G
Space group	*Pmmm* (47)	*Ama*2 (40)	$P2_1/m$ (11)	*Cmmm* (65)
Non-Mag.	325.5	144.8	142.5	0
DP (LDA)	A	C1	C2	G
Energy	366.2	412.7	469.2	0
DP (LDA)	D-1	D-2	D-3	–
Energy	341.69	476.7	341.8	–
RP (LDA)	A	C1	C2	G
Non-Mag.	422.56	190.6	185.2	0

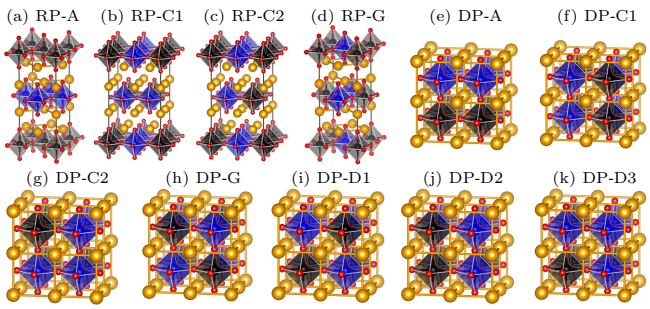


Fig. 1. Possible crystal structures of panels (a)–(d) Ruddlesden–Popper (RP) $Sr_2Fe_{0.5}Ru_{0.5}O_4$ and panels (e)–(k) double perovskite (DP) $SrFe_{0.5}Ru_{0.5}O_3$. (a) RP-A, (b) RP-C1, (c) RP-C2, (d) RP-G, (e) DP-A, (f) DP-C1, (g) DP-C2, (h) DP-G, (i) DP-D1, (j) DP-D2, (k) DP-D3. The Sr, Fe, Ru and O atoms are labeled by yellow, black, blue and red balls, respectively.

3.2. Electronic properties

Using the DFT-optimized ground state structures of DP $SrFe_{0.5}Ru_{0.5}O_3$ (Fig. 1(h)) and RP $Sr_2Fe_{0.5}Ru_{0.5}O_4$ (Fig. 1(d)), we proceed to calculate the (non-spin-polarized) band structure and DOS, as presented in Figs. 2 and 3, respectively. In the case of DP $SrFe_{0.5}Ru_{0.5}O_3$, as depicted in Fig. 2(a), the Fe-d orbitals exhibit a relatively smaller crystal field splitting between the t_{2g} and e_g orbitals. In comparison to Ru-4d orbitals, Fe-3d orbitals are more localized and experience less repulsion from the oxygen (O) ligands. The on-site hopping terms of Fe-t_{2g}, Fe-e_g, Ru-t_{2g}, and Ru-e_g, which are obtained from Wannier projections, are determined as −0.421 eV, 1.661 eV, −0.264 eV, and 3.052 eV, respectively. Consequently, the crystal field splitting (Δ) between t_{2g} and e_g for Fe and Ru is calculated as 2.082 eV and 3.316 eV, respectively. The smaller Δ for Fe leads to electronic occupations at e_g orbitals, this results in the formation of a high-spin Fe state under strong Hund's exchange J. In contrast, the larger Δ for Ru leaves the Ru-t_{2g} states near the Fermi surface (E_f: 0 eV) while the e_g states are located at higher energies ranging from 2.5 eV to 5.0 eV (as shown in the bottom panel of Fig. 3(a)). The DOS in Fig. 3(a) demonstrates hybridization between Fe-t_{2g} and Ru-t_{2g} orbitals, forming a hybridized peak slightly above E_f. Additionally, a broader hybridization peak is observed between Fe-e_g and Ru-e_g orbitals within the energy range from 0 to 2 eV. The hybridization with Fe-3d effectively reduces the bandwidth of Ru-4d orbitals, as evidenced by the reduced bandwidth ($\sim$ 2.5 eV) of Ru-t_{2g} compared to $\sim$ 3.2 eV bandwidth in bulk $SrRuO_3$. This reduction in bandwidth plays a crucial role in enhancing electronic correlations and resulting in significant spin-splitting, as discussed in the next section.

Please note that in the non-spin-polarized DOS of the G-type DP $SrFe_{0.5}Ru_{0.5}O_3$ (Fig. 3(a)), the e_g orbitals of both Fe and Ru are mostly unoccupied, and no significant charge transfer is observed. This indicates that both Ru and Fe are close to their nominal d^4 state. The DOS of DP $SrFe_{0.5}Ru_{0.5}O_3$ exhibits similarities with Sr_2CrRuO_6,[62] with the only difference being that the Cr-d orbitals are occupied by three electrons instead of five in Fe-d orbitals.

In the case of G-type RP $Sr_2Fe_{0.5}Ru_{0.5}O_4$, the inter-layer hopping along the z-direction is eliminated due to the layered crystal structure of Ruddlesden–Popper phase. This is evidenced by the DOS of Fe-d_{z^2} and Ru-d_{z^2} shown in the bottom panel of Fig. 3(b). For RP $Sr_2Fe_{0.5}Ru_{0.5}O_4$, the bandwidth of d_{xz}/d_{yz} and d_{z^2} orbitals for both Fe and Ru is significantly reduced compared to that of DP $SrFe_{0.5}Ru_{0.5}O_3$, resulting from the layered structure of the material.

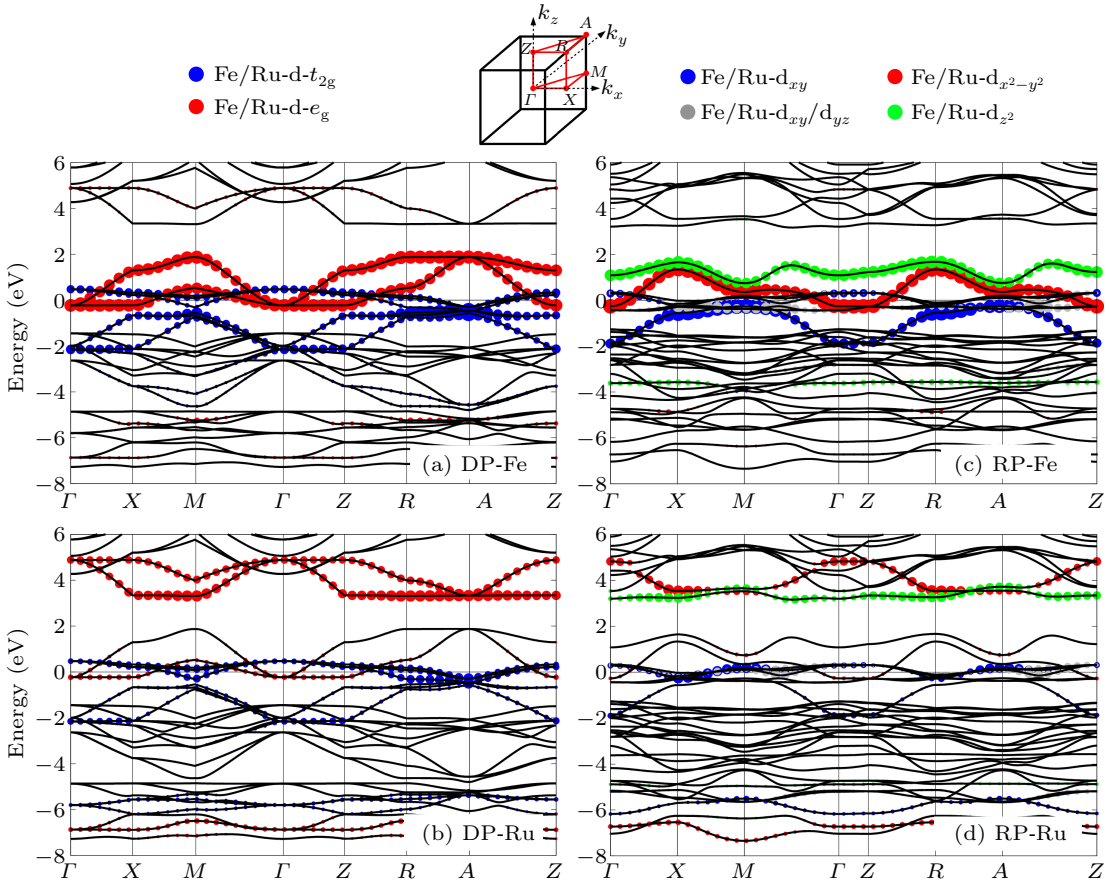


Fig. 2. DFT non-magnetic band characters structure of (a) and (b) DP-type $SrFe_{0.5}Ru_{0.5}O_3$ and (c) and (d) RP-type $Sr_2Fe_{0.5}Ru_{0.5}O_4$. The k-path for band plotting is shown in the upper panel. The dots with different sizes and colors demonstrate the atoms' and orbitals' contributions to the total band structure, the legends are shown in the upper panels of (a) and (c).

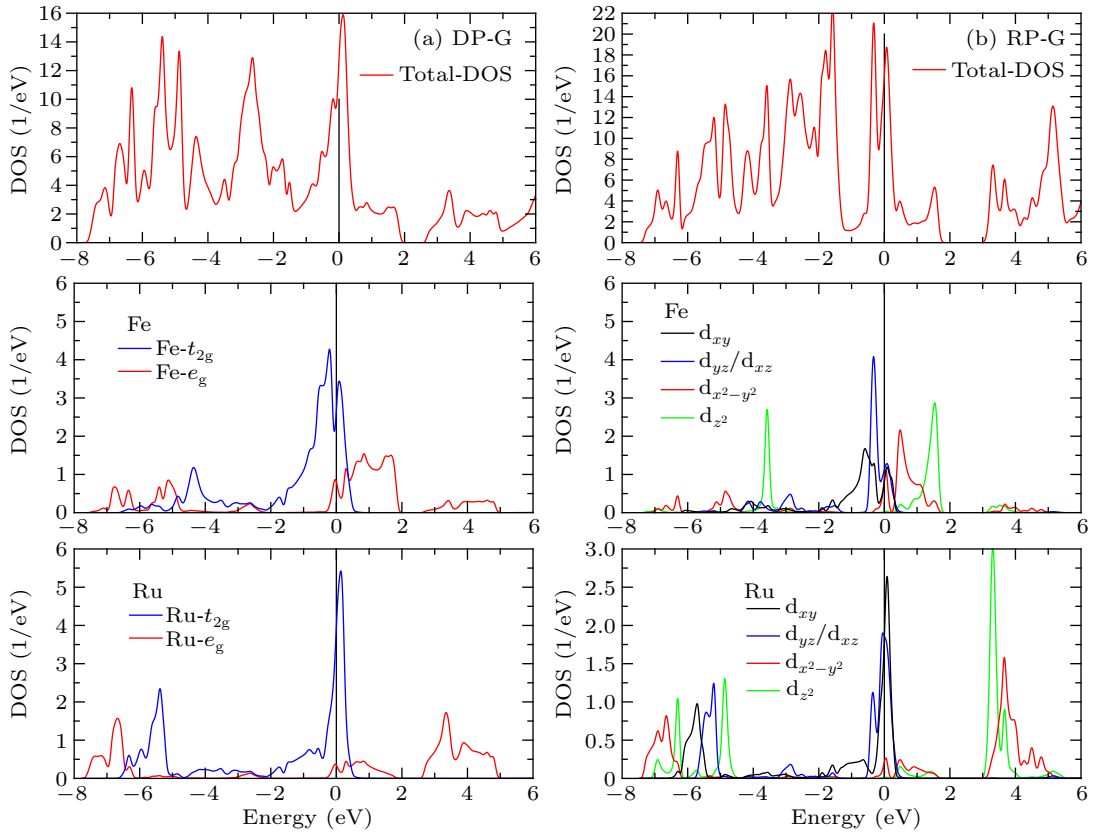


Fig. 3. DFT non-magnetic density of states (DOS) of (a) DP-type $SrFe_{0.5}Ru_{0.5}O_3$ and (b) RP-type $Sr_2Fe_{0.5}Ru_{0.5}O_4$. To demonstrate the orbital localization and band splitting of Ru-4d and Fe-3d orbitals, the atomic- and orbital-resolved DOS are also shown.

3.3. Magnetic properties

We proceed to investigate the magnetic properties of DP $SrFe_{0.5}Ru_{0.5}O_3$ and RP $Sr_2Fe_{0.5}Ru_{0.5}O_4$ by calculating the spin-polarized DFT + U (U: Coulomb interaction) total energies for all possible magnetic orders. Figures 4(a)–4(d) and 4(e)–4(h) depict the potential magnetic states of DP $SrFe_{0.5}Ru_{0.5}O_3$ and RP $Sr_2Fe_{0.5}Ru_{0.5}O_4$, respectively. The DFT + U total energies of all magnetic orders are presented in Table 2. In the case of DP $SrFe_{0.5}Ru_{0.5}O_3$, the A-type (AFM-A) and C-type (AFM-C) antiferromagnetic orders converge to non-magnetic states during self-consistent DFT + U iterations, indicating their instability. However, the ferromagnetic (FM) and G-type (AFM-G) states successfully converge. It is important to note that since the magnetic moments on Ru and Fe are not equal, approximately $5\mu_B$/Fe and $3\mu_B$/Ru, the AFM-G state is essentially a ferrimagnetic (FIM) state with a net magnetic moment of $(5-3)/2 = 1.0\mu_B$ per $SrFe_{0.5}Ru_{0.5}O_3$.

Table 2 reveals that the FIM state (Fig. 4(d)) is the ground state with the lowest energy while the FM state (Fig. 4(a)) is a metastable state with an energy 151.1 meV higher than the FIM state. By fitting the total energies of the FM and FIM states into a simple 3D Heisenberg model, we estimate that the nearest exchange energy ($J_{\text{inter-site}}$) between Ru and Fe is approximately 13 meV. This suggests a potentially high magnetic transition (Néel) temperature in the range of several hundred Kelvin. These findings for DP $SrFe_{0.5}Ru_{0.5}O_3$, specifically the FIM magnetic state, align with experimental results reported in Ref. [40], which reported a room-temperature FIM state in the double perovskite Sr_2FeRuO_6 that is isochemically identical to DP $SrFe_{0.5}Ru_{0.5}O_3$. Additionally, both the FM and FIM states exhibit an insulating behavior with a non-zero band gap. It is expected that an external magnetic field could induce a spin flip from the antiferromagnetically coupled Ru and Fe to ferromagnetically coupled pairs, leading to a reduction in electric resistance. Therefore, DP $SrFe_{0.5}Ru_{0.5}O_3$ holds promise for exhibiting the magnetoresistance effect.

In the case of RP $Sr_2Fe_{0.5}Ru_{0.5}O_4$, we categorize the possible magnetic orders based on the intra-layer AFM/FM and intra-layer FM/AFM couplings: FM (intra-layer FM + inter-layer FM), FIM (intra-layer AFM + inter-layer FM), AFM-A (intra-layer FM + inter-layer AFM), and AFM-G (intra-layer AFM + inter-layer AFM). By performing spin-polarized DFT + U calculations, we find that the ground state is the FIM state (its energy is set as 0) while the metastable state is the AFM-G state with an energy of 2.2 meV. This indicates that the magnetism of RP $Sr_2Fe_{0.5}Ru_{0.5}O_4$ is primarily governed by a strong intra-layer AFM coupling between Fe and Ru ($J_{\text{inter-site}} \sim 7$ meV), along with a much weaker inter-layer coupling ($J_{\text{inter-layer}} \sim 1$ meV). The reduced value of $J_{\text{inter-site}}$ can be attributed to the cutting-off of hopping interactions along the out-of-plane direction (z). In DP $SrFe_{0.5}Ru_{0.5}O_3$, the $J_{\text{inter-site}}$ value is approximately 13 meV, which is stronger due to its three-dimensional (3D) nature. In contrast, in RP $Sr_2Fe_{0.5}Ru_{0.5}O_4$, the hopping along the z-direction is hindered by the layered structure, resulting in a $J_{\text{inter-site}}$ value of roughly half of DP $SrFe_{0.5}Ru_{0.5}O_3$, approximately 7 meV.

Table 2. Total energies, total and atom projected magnetic moment, and magnetic point and space group in the Hermann–Mauguin notation (generated by FINDSYM[65]) of different magnetic orders (including ferromagnetic: FM; A-, C- and G-type antiferromagnetic: AFM-A, AFM-C, AFM-G; for DP phase, the AFM-G order is equivalent to FIM order) of DP $SrFe_{0.5}Ru_{0.5}O_3$ and RP $Sr_2Fe_{0.5}Ru_{0.5}O_4$ computed by DFT + U method, the energy unit is in meV of per $2\times2\times2$ supercell of $SrFe_{0.5}Ru_{0.5}O_3$ (e.g., Figs. 1(e)–1(k)) and $2\times2\times1$ supercell of $Sr_2Fe_{0.5}Ru_{0.5}O_4$ (Figs. 1(a) and 1(d)), respectively. The moment unit is μ_B per $SrFe_{0.5}Ru_{0.5}O_3$ and $Sr_2Fe_{0.5}Ru_{0.5}O_4$. For the schematic pattern of different magnetic orders see Fig. 4. The temperatures in brackets are Néel of FIM orders computed by DMFT.

DP (GGA-PS)	FM	AFM-A	AFM-C	AFM-G (FIM)
Magnetic point (space) group	422 (*I*4*mm*)	4*mm* (*P*4/*nmm*)	4*mm* (*P*4/*nmm*)	422 (*I*4*mm*)
Energy	151.1	–	–	0
Moment (total)	4.0	–	–	1.0
Moment (Fe)	4.3	–	–	4.3
Moment (Ru)	2.3	–	–	−1.9
RP (GGA-PS)	**FM**	**FIM**	**AFM-A**	**AFM-G**
Magnetic point (space) group	*mm*2 (*Amm*2)	*mm*2 (*Amm*2)	*mmm* (*Pmma*)	*mmm* (*Pmma*)
Energy	58.2	0	49.5	2.2
Moment (total)	4.0	1.0	0	2.2
Moment (Fe)	4.2	4.2	±4.2	±4.2
Moment (Ru)	2.2	–1.9	±2.2	±1.9

The negligible inter-layer coupling with $J_{\text{inter-layer}}$ approximately 1 meV corresponds to a temperature of only around 11 K. This suggests that the coexistence of the FIM and AFM-G states is possible, where local strain or crystal disorder in realistic samples could locally stabilize one state in certain regions. Additionally, the application of an external magnetic field is expected to facilitate the transformation from the AFM-G to the FIM state. Consequently, the resistance can be effectively reduced, similar to DP $SrFe_{0.5}Ru_{0.5}O_3$. Therefore, RP $Sr_2Fe_{0.5}Ru_{0.5}O_4$ holds promise as a candidate for magnetoresistance effects.

We also perform similar magnetic order calculations including spin–orbital coupling (SOC) in calculations. With SOC, non-collinear magnetic order setups are allowed and they might lead to lower energy compared with the collinear magnetic order as shown in Figs. 4(d) and 4(h). We test different combinations by changing the magnetic orientations of Fe- and Ru-moment, e.g., by allowing their magnetic moment along (001), (010), (001), (110), (111) and other possible directions. However, our DFT + U + SOC results demonstrate that collinear G-type orders with both Fe- and Ru-

moment along z (001) direction are ground states for both $SrFe_{0.5}Ru_{0.5}O_3$ and $Sr_2Fe_{0.5}Ru_{0.5}O_4$, as shown in Figs. 4(d) and 4(h).

Our findings reveal the following: (i) DP $SrFe_{0.5}Ru_{0.5}O_3$ exhibits a robust G-type structure and a semiconducting state with a FIM order. (ii) RP $Sr_2Fe_{0.5}Ru_{0.5}O_4$ possesses a G-type structure with a strong intra-layer FIM order and a weak intra-layer coupling of approximately 1 meV. This suggests that the FIM and AFM-G configurations have similar energies, indicating a significant magnetic competition among various magnetic states. This competition may give rise to phenomena such as spin-glass behavior,[66] spin-density waves,[27] or commensurate/incommensurate magnetic ordering.[28] Moreover, this could explain the experimentally observed uncertain magnetism in Fe-doped ruthenates.[27,28,66]

We proceed with the calculation of the spin-polarized DOS for DP $SrFe_{0.5}Ru_{0.5}O_3$ and RP $Sr_2Fe_{0.5}Ru_{0.5}O_4$. Figures 5(a) and 5(b) illustrate the DOS of DP $SrFe_{0.5}Ru_{0.5}O_3$ and RP $Sr_2Fe_{0.5}Ru_{0.5}O_4$, respectively. In the case of DP $SrFe_{0.5}Ru_{0.5}O_3$, the Fe dopant atoms are in the Fe^{3+} state with a $3d^5$ electronic configuration, as indicated by the fully occupied spin-majority Fe-t_{2g} and e_g orbitals (middle panel of Fig. 5(a)). The full spin polarization at Fe and the Fe^{3+} valence states are consistent with those observed in Sr_2FeMoO_6.[67]

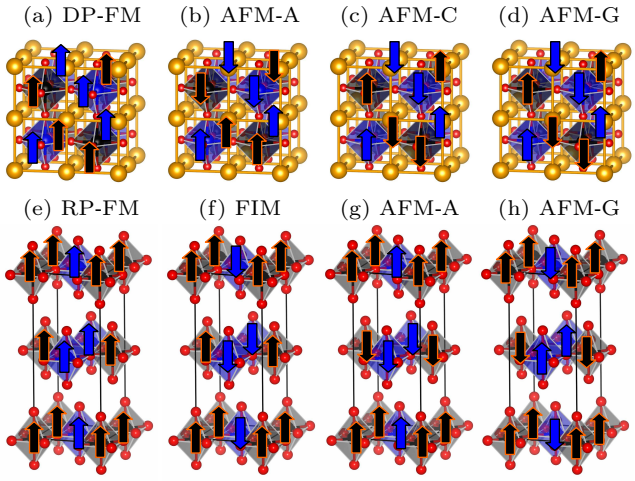


Fig. 4. Possible magnetic orders for (a)–(d) DP-type $SrFe_{0.5}Ru_{0.5}O_3$ and (e)–(h) RP-type $Sr_2Fe_{0.5}Ru_{0.5}O_4$. For $Sr_2Fe_{0.5}Ru_{0.5}O_4$, Sr atoms are not plotted for simplification. The black and blue arrows indicate the (spin up and down) moments on Fe and Ru, respectively.

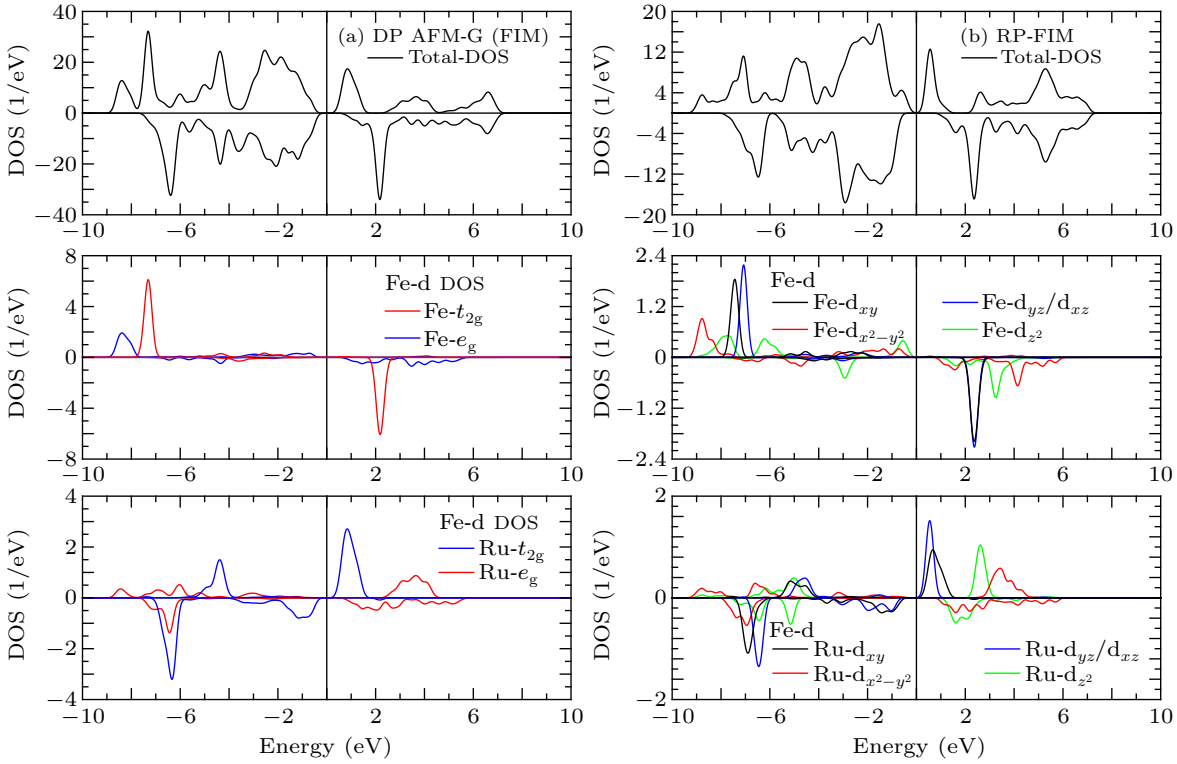


Fig. 5. DFT + U spin-polarized density of states of (a) DP S and (b) RP $Sr_2Fe_{0.5}Ru_{0.5}O_4$. To demonstrate the orbital localization and band splitting of Ru-4d and Fe-3d orbitals, the atomic- and orbital-resolved DOS are also shown. The positive and negative values of these DOS indicate spin-up and spin-down channels, respectively.

It is worth noting that in the spin-polarized DOS of both compounds (Figs. 5(a) and 5(b)), the states near the Fermi level (E_f) are not predominantly composed of hybridized states between Fe and Ru. This suggests a weaker hybridization compared to the non-spin-polarized DOS shown in Figs. 3(a) and 3(b). Fe exhibits a strong spin splitting of approximately 8 eV, which is significantly larger than the values of around 2.5 eV for Fe in Sr_2FeMnO_6,[67] 3.5 eV for Cr in Sr_2CrRuO_6,[62] and 2.0 eV for Cr in Sr_2CrMoO_6.[68] Additionally, the spin splitting of Ru-t_{2g} in DP $SrFe_{0.5}Ru_{0.5}O_3$ is

approximately 7 eV, almost three times larger than that in bulk $SrRuO_3$, which is around 2 eV.[48] This indicates that the reduced electronic hoppings and decreased itinerancy make both Fe and Ru more localized compared to their bulk states in $SrFeO_3$ and $SrRuO_3$. Consequently, a larger intrinsic magnetic moment develops at the Fe and Ru sites. Due to the weaker hybridization between Fe and Ru in the spin-polarized state, the superexchange interaction between the magnetic Fe and Ru ions is enhanced because it is proportional to the spin moment on Fe and Ru. Along with the half-metallic state exhibited in DP $SrFe_{0.5}Ru_{0.5}O_3$, the superexchange mechanism consequently appears to play an essential role in stabilizing the FIM order.

The DOS of RP $Sr_2Fe_{0.5}Ru_{0.5}O_4$ exhibits notable similarities to that of DP $SrFe_{0.5}Ru_{0.5}O_3$. For example, the spin-up Fe-t_{2g} states are located around -7 eV, while the spin-down Fe-t_{2g} states are at approximately 2 eV. Similarly, the spin-up Ru-d_{yz}/d_{xz} states are observed around -6 eV, and the spin-down states are found at around 1 eV. The layered structure of RP $Sr_2Fe_{0.5}Ru_{0.5}O_4$ leads to a splitting between the degenerate t_{2g} and e_g orbitals. These findings suggest that Fe-doped ruthenates share similarities with Sr_2CrMoO_6,[68] such as weakened 3d–4d hybridization and the significant role of superexchange in stabilizing the FIM order.

3.4. Dynamical correlation effects

To investigate the temperature effect, we employ the DMFT method, as DFT is a zero-temperature theory. We consider two different Hamiltonians, Kanamori and density–density interactions, at temperatures of 200 K and 300 K. The DMFT calculations confirm the presence of FIM order in DP $SrFe_{0.5}Ru_{0.5}O_3$ and RP $Sr_2Fe_{0.5}Ru_{0.5}O_4$, respectively, consistent with the results obtained from DFT + U calculations. Figure 6 displays the Kanamori DMFT spectra of DP $SrFe_{0.5}Ru_{0.5}O_3$ and RP $Sr_2Fe_{0.5}Ru_{0.5}O_4$ at room temperature ($T = 300$ K). In DP $SrFe_{0.5}Ru_{0.5}O_3$, the Fe and Ru atoms are antiferromagnetically coupled, with the spin-majority channel being spin-up for Fe and spin-down for Ru. The spin-up t_{2g} and e_g orbitals of Fe are fully occupied while the spin-down t_{2g} and e_g orbitals are only slightly occupied, indicating a high-spin Fe^{3+} ($3d^5$) state. As for Ru, the spin-down t_{2g} orbitals are occupied while the spin-down e_g orbital and other states in the spin-up channel are all empty, indicating a high-spin Ru^{5+} ($4d^3$) state. The magnetic moment per $SrFe_{0.5}Ru_{0.5}O_3$ in the DP phase is approximately $1\mu_B$ at 300 K. In RP $Sr_2Fe_{0.5}Ru_{0.5}O_4$, the DMFT spectra exhibit remarkable similarities to those of DP $SrFe_{0.5}Ru_{0.5}O_3$, with the only difference being the degeneracy splitting within the t_{2g} and e_g orbitals. Specifically, the d_{xy} ($d_{x^2-y^2}$) orbital is not symmetric to the d_{yz} and d_{z^2} orbitals as observed in DP $SrFe_{0.5}Ru_{0.5}O_3$. These DMFT results indicate that the magnetism in both systems is expected to persist even at room temperature. To make summary, the magnetic exchange parameters from DFT + U, and Néel that is estimated from magnetic exchange parameters J and computed from DMFT as shown in Table 3, one can see that the values from DMFT are definitely higher than the estimated values from J, indicating possible important roles of correlation effects in Fe-doped ruthenates. Additionally, we also compute the net magnetic moments using the density–density interactions, and it is found that the net moments of both systems increased by 10%, highlighting the significance of Hund's exchange interaction (J).

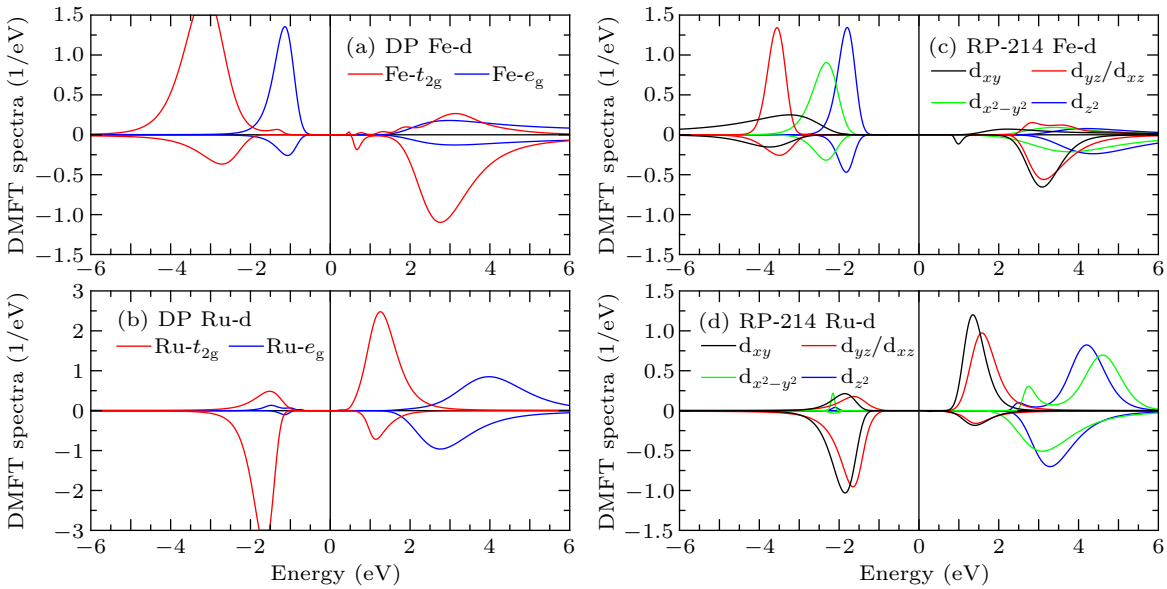


Fig. 6. DMFT spectra of (a)–(b) (DP) $SrFe_{0.5}Ru_{0.5}O_3$ and (c)–(d) (RP) $Sr_2Fe_{0.5}Ru_{0.5}O_4$ at $T = 300$ K. The upper and bottom panels show the spectra of Fe and Ru, respectively. The spin-up and -down spectra are shown as positive and negative values, respectively.

Table 3. Magnetic exchange parameters (per chemical formula) calculated by DFT + U, and Néel temperatures estimated by exchange parameters and DMFT calculations.

–	Exchange parameters (meV)	Néel (exchange parameters)	Néel (DMFT)
DP FIM	$J_{\text{inter-site}}$: 13	$\sim$ 151 K	$>$ 500 K
RP AFM-G (FIM)	$J_{\text{inter-site}}$: 7	$\sim$ 81 K	$>$ 300 K
–	$J_{\text{inter-layer}}$: 1	–	–

Note that the ruthenates we have studied in this paper are all at exactly 50% Fe-doping, however, crystal and lattice defects, as well as inter-atomic mixing, and even the formation of oxygen vacancies, are usually unavoidable in practical experiments. For oxides, the above types of crystal defects, as well as oxygen vacancies, are expected to induce doping of electrons or holes. Any additional electron or hole doping will close to the Mott band gap, leading to the formation of metallic phases. Moreover, this will, to some extent, increase the double-exchange interaction of the system, and we expect that a moderate amount of hole or electron doping will enhance the double-exchange interaction while decreasing the strong electronic correlation effects at Ru and Fe as well as the superexchange interaction, which will likely lead to the transition of both the Fe-doped ruthenates from FIM to FM state.[69–71]

4. Conclusion

Motivated by the potential for exotic physical properties induced by Fe-doping in ruthenates, we conducted a comprehensive study on the structural, electronic, and magnetic properties of Fe-doped double perovskite $SrRuO_3$ and Ruddlesden–Popper Sr_2RuO_4, specifically $SrFe_{0.5}Ru_{0.5}O_3$ and $Sr_2Fe_{0.5}Ru_{0.5}O_4$. TMOs with 3d electrons often exhibited remarkable magnetic properties around room temperature, and thus, we anticipated that Fe-doping would enhance the magnetic performance of $SrRuO_3$ and Sr_2RuO_4 by raising the Curie or Néel temperatures.

Our investigations reveal that the Fe atoms tend to segregate, leading to the formation of G-type structure with Fe and Ru atoms in both $SrFe_{0.5}Ru_{0.5}O_3$ and $Sr_2Fe_{0.5}Ru_{0.5}O_4$. These compounds adopt a double-perovskite-type three-dimensional (3D) and two-dimensional (2D) structure, respectively. The interplay between weakened 3d–4d hybridization, enlarged spin-splitting, and enhanced correlation effects results in a substantial charge transfer from Ru to Fe, resulting in Fe^{3+} and Ru^{5+} states. The superexchange interaction between Fe^{3+} and Ru^{5+} ions gives rise to a robust FIM semiconducting ground state in both systems. By considering dynamical correlation effects, band gaps of up to 2 eV are observed.

Due to their FIM ground states, significant spin-flip behavior is expected under the influence of a strong external magnetic field, implying the potential for remarkable magnetoresistance effects. To investigate the survival of the FIM states in $SrFe_{0.5}Ru_{0.5}O_3$ and $Sr_2Fe_{0.5}Ru_{0.5}O_4$ at higher temperatures, we perform temperature-dependent DMFT calculations. The results demonstrate that the FIM states persist even at elevated temperatures, including room temperature (300 K). The ability to stabilize semiconducting FIM states through Fe doping in $SrRuO_3$ and Sr_2RuO_4 renders Fe doping a promising strategy for overcoming the limitations of working and operating temperatures in 4d transition metal oxides such as ruthenates.

Acknowledgments

Project supported by the starting funds from Northwest University. We thank Paul Worm and Karsten Held for fruitful discussion and support of computational resources. Calculations have been mainly done on the Vienna Scientific Clusters (VSC) and supercomputer at the School of Physics of Northwest University.

References

[1] Green M A, Ho-Baillie A and Snaith H J 2014 *Nat. Photonics* **8** 506
[2] Hwang J, Rao R R, Giordano L, Katayama Y, Yu Y and Shao-Horn Y 2017 *Science* **358** 751
[3] Anderson P W, Baskaran G, Zou Z and Hsu T 1987 *Phys. Rev. Lett.* **58** 2790
[4] Mulder A T, Benedek N A, Rondinelli J M and Fennie C J 2013 *Adv. Funct. Mater.* **23** 4810
[5] Birol T, Benedek N A and Fennie C J 2011 *Phys. Rev. Lett.* **107** 257602
[6] Kim B J, Ohsumi H, Komesu T, Sakai S, Morita T, Takagi H and Arima T H 2009 *Science* **323** 1329
[7] Kim B J, Jin H, Moon S J, Kim J Y, Park B G, Leem C S, Yu J, Noh T W, Kim C, Oh S J, Park J H, Durairaj V, Cao G and Rotenberg E 2008 *Phys. Rev. Lett.* **101** 076402
[8] Koster G, Klein L, Siemons W, Rijnders G, Dodge J S, Eom C B, Blank D H A and Beasley M R 2012 *Rev. Mod. Phys.* **84** 253
[9] Mackenzie A P and Maeno Y 2003 *Rev. Mod. Phys.* **75** 657
[10] Fang Z, Nagaosa N, Takahashi K S, Asamitsu A, Mathieu R, Ogasawara T, Yamada H, Kawasaki M, Tokura Y and Terakura K 2003 *Science* **302** 92
[11] Meng K Y, Ahmed A S, Bacani M, *et al.* 2019 *Nano Lett.* **19** 3169
[12] Matsuno J, Ogawa N, Yasuda K, Kagawa F, Koshibae W, Nagaosa N, Tokura Y and Kawasaki M 2016 *Sci. Adv.* **2** e1600304
[13] Wang L, Feng Q, Kim Y, *et al.* 2018 *Nat. Mater.* **17** 1087
[14] Lu J, Si L, Zhang Q, *et al.* 2021 *Adv. Mater.* **33** 2102525
[15] Nelson K, Mao Z, Maeno Y and Liu Y 2004 *Science* **306** 1151
[16] Kallin C 2012 *Rep. Prog. Phys.* **75** 042501
[17] Ishida K, Mukuda H, Kitaoka Y, *et al.* 1998 *Nature* **396** 658
[18] Luke G, Fudamoto Y, Kojima K, *et al.* 1998 *Nature* **394** 558
[19] Rice T and Sigrist M 1995 *J. Phys.: Condens. Mat.* **7** L643
[20] Cao M, Liu T, Gao S, Sun G, Wu X, Hu C and Wang Z L 2005 *Angew. Chem.* **117** 4269
[21] Stolen S, Gronvold F, Brinks H, Atake T and Mori H 1998 *J. Chem. Thermodyn.* **30** 365
[22] Matsumoto G 1970 *J. Phys. Soc. Jpn.* **29** 606
[23] Swarnkar A, Mir W J and Nag A 2018 *ACS Energy Lett.* **3** 286
[24] Long Y, Hayashi N, Saito T, Azuma M, Muranaka S and Shimakawa Y 2009 *Nature* **458** 60
[25] Kunkemöller S, Nugroho A A, Sidis Y and Braden M 2014 *Phys. Rev. B* **89** 045119
[26] Braden M, Friedt O, Sidis Y, Bourges P, Minakata M and Maeno Y 2002 *Phys. Rev. Lett.* **88** 197002

[27] Ortmann J, Liu J, Hu J, Zhu M, Peng J, Matsuda M, Ke X and Mao Z 2013 *Sci. Rep.* **3**

[28] Zhu M, Shanavas K V, Wang Y, Zou T, Sun W F, Tian W, Garlea V O, Podlesnyak A, Matsuda M, Stone M B, Keavney D, Mao Z Q, Singh D J and Ke X 2017 *Phys. Rev. B* **95** 054413

[29] Hicks C W, Brodsky D O, Yelland E A, *et al.* 2014 *Science* **344** 283

[30] NishiZaki S, Maeno Y and Mao Z 2000 *J. Phys. Soc. Jpn.* **69** 572

[31] Deguchi K, Mao Z Q, Yaguchi H and Maeno Y 2004 *Phys. Rev. Lett.* **92** 047002

[32] Fan J, Liao S, Wang W, *et al.* 2011 *J. Appl. Phys.* **110** 043907

[33] Bansal C, Kawanaka H, Takahashi R and Nishihara Y 2003 *J. Alloys Compd.* **360** 47

[34] Kikugawa N, Mackenzie A P, Bergemann C, Borzi R A, Grigera S A and Maeno Y 2004 *Phys. Rev. B* **70** 060508

[35] Kikugawa N, Bergemann C, Mackenzie A P and Maeno Y 2004 *Phys. Rev. B* **70** 134520

[36] Qasim I, Blanchard P E, Liu S, Tang C, Kennedy B J, Avdeev M and Kimpton J A 2013 *J. Solid State Chem.* **206** 242

[37] Shen K M, Kikugawa N, Bergemann C, Balicas L, Baumberger F, Meevasana W, Ingle N J C, Maeno Y, Shen Z X and Mackenzie A P 2007 *Phys. Rev. Lett.* **99** 187001

[38] Zhong Z and Hansmann P 2017 *Phys. Rev. X* **7** 011023

[39] Chen H and Millis A 2017 *J. Phys.: Condens. Matter* **29** 243001

[40] Chang J, Lee K, Jung M H, Kwon J H, Kim M and Kim S K 2011 *Chem. Mater.* **23** 2693

[41] Kresse G and Hafner J 1993 *Phys. Rev. B* **47** 558

[42] Kresse G and Furthmüller J 1996 *Comput. Mater. Sci.* **6** 15

[43] Blaha P, Schwarz K, Madsen G, Kvasnicka D and Luitz J 2001 *An augmented plane wave+ local orbitals program for calculating crystal properties*

[44] Schwarz K, Blaha P and Madsen G K H 2002 *Comput. Phys. Commun.* **147** 71

[45] Perdew J P, Ruzsinszky A, Csonka G I, Vydrov O A, Scuseria G E, Constantin L A, Zhou X and Burke K 2008 *Phys. Rev. Lett.* **100** 136406

[46] Anisimov V I, Zaanen J and Andersen O K 1991 *Phys. Rev. B* **44** 943

[47] Liechtenstein A I, Anisimov V I and Zaanen J 1995 *Phys. Rev. B* **52** R5467

[48] Miyake T and Aryasetiawan F 2008 *Phys. Rev. B* **77** 085122

[49] Si L, Zhong Z, Tomczak J M and Held K 2015 *Phys. Rev. B* **92** 041108

[50] Li Z, Iitaka T and Tohyama T 2012 *Phys. Rev. B* **86** 094422

[51] Li Z, Laskowski R, Iitaka T and Tohyama T 2012 *Phys. Rev. B* **85** 134419

[52] Wannier G H 1937 *Phys. Rev.* **52** 191

[53] Marzari N, Mostofi A A, Yates J R, Souza I and Vanderbilt D 2012 *Rev. Mod. Phys.* **84** 1419

[54] Mostofi A A, Yates J R, Lee Y S, Souza I, Vanderbilt D and Marzari N 2008 *Comput. Phys. Commun.* **178** 685

[55] Kune J, Arita R, Wissgott P, Toschi A, Ikeda H and Held K 2010 *Comput. Phys. Commun.* **181** 1888

[56] Gull E, Millis A J, Lichtenstein A I, Rubtsov A N, Troyer M and Werner P 2011 *Rev. Mod. Phys.* **83** 34910

[57] Parragh N, Toschi A, Held K and Sangiovanni G 2012 *Phys. Rev. B* **86** 155158

[58] Wallerberger M, Hausoel A, Gunacker P, Kowalski A, Parragh N, Goth F, Held K and Sangiovanni G 2019 *Comput. Phys. Commun.* **235** 388

[59] Kaufmann J and Held K 2023 *Comput. Phys. Commun.* **282** 108519

[60] Gubernatis J E, Jarrell M, Silver R N and Sivia D S 1991 *Phys. Rev. B* **44** 6011

[61] Sandvik A W 1998 *Phys. Rev. B* **57** 10287

[62] Halder A, Sanyal P and Saha-Dasgupta T 2019 *Phys. Rev. B* **99** 020402

[63] Nowik I and Felner I 2004 *Hyperfine Interact.* **156** 195

[64] Battle P, Gibb T, Jones C and Studer F 1989 *J. Solid State Chem.* **78** 281

[65] Stokes H T and Hatch D M 2005 *J. Appl. Crystallogr.* **38** 237

[66] Zhu M, Wang Y, Li P G, Ge J J, Tian W, Keavney D, Mao Z Q and Ke X 2017 *Phys. Rev. B* **95** 174430

[67] Sarma D D, Mahadevan P, Saha-Dasgupta T, Ray S and Kumar A 2000 *Phys. Rev. Lett.* **85** 2549

[68] Sanyal P, Halder A, Si L, Wallerberger M, Held K and Saha-Dasgupta T 2016 *Phys. Rev. B* **94** 035132

[69] Pan H, Yi J B, Shen L, Wu R Q, Yang J H, Lin J Y, Feng Y P, Ding J, Van L H and Yin J H 2007 *Phys. Rev. Lett.* **99** 127201

[70] Wang X, Song Y, Tao L L, Feng J F, Sui Y, Tang J, Song B, Wang Y, Wang Y, Zhang Y and Han X F 2014 *Appl. Phys. Lett.* **105** 262402

[71] Hua E, Si L, Dai K, Wang Q, Ye H, Liu K, Zhang J, Lu J, Chen K, Jin F, Wang L and Wu W 2014 *Adv. Mater.* **34** 2270327